J Mater Sci (2008) 43:4607–4617
DOI 10.1007/s10853-008-2677-z

Electrical conductivity enhancement of a polymer using butyl glycidyl ether (BGE)–lithium hexafluorophosphate ($LiPF_6$) complex

Soumen Jana · Wei-Hong Zhong

Received: 16 January 2008 / Accepted: 25 April 2008 / Published online: 13 May 2008

Abstract In this study, we investigated the improvement in electrical conductivity of a polymer with the addition of dissolved lithium hexafluorophosphate ($LiPF_6$) in an ether based solvent, butyl glycidyl ether (BGE). Thin film samples were fabricated by adding $LiPF_6$ (up to 1 wt%) to poly (methyl-methacrylate) (PMMA). Film with 0.75% $LiPF_6$ showed the highest improvement of electrical conductivity by three orders of magnitude. Both FTIR spectra and X-ray diffraction studies confirmed the formation of BGE–$LiPF_6$ complex. Differential Scanning Calorimetry was used to characterize the PMMA/$LiPF_6$ specimens further. Dielectric experiments revealed the existence of multiple composition dependent relaxation processes: β (high frequency) and β (low frequency) relaxation processes. The results suggest that electrical conductivity could be improved without influencing the domain polymer and the composite materials, including their processability. This work suggests that the conductivity of nanocomposites with various solid conductive fillers may be sufficiently enhanced in combination with this ion conduction approach involving a "liquid conductive filler." Since BGE is compatible with epoxy molecules, further study is expected to lead to an effective solution to conductive epoxy composites in their wide field of applications including aircraft and multifunctional energy sources such as structural batteries.

S. Jana · W.-H. Zhong (✉)
School of Mechanical and Materials Engineering,
Washington State University, Pullman, WA 99164, USA
e-mail: Katie_Zhong@wsu.edu

Introduction

Electrically conductive polymeric materials have found increasing applications in many industries. Improvements in electrical conductivity of a polymer could be realized by either addition of solid conductive particles, such as carbon nanotubes, carbon fibers, and/or metal particles, or addition of alkali metal salts through increments of ionic conductivity of the polymer at ambient temperature [1, 2]. Although numerous research has been conducted on the enhancement in conductivity through making nanocomposites with those conductive nano-fillers, development of novel polymeric materials with alkali metal salt, similar to solid electrolytes, are also attractive due to potential applications of enhancement of macroscopic properties including electrical and thermal properties, as well as chemical stability and easy processability [3–11].

Among different alkali metallic salts, Lithium hexafluorophosphate ($LiPF_6$) is being used extensively as a solute for lithium salt based polymer electrolyte. Additions of ether in both solid and liquid electrolytes systems which contain alkali metal salts influence the electrochemical properties of the systems [12–16]. Oxyethylene units ($–CH_2–CH_2–O–$) with its high coordination affinities to alkali metal ions show strong effects on ion mobility [17]. Much of this type of work is related to poly (ethylene oxide) (PEO), which provides oxygen to make coordination with Li^+ cation. The goal of this work is to explore the potential that this kind of coordination formation could be used to increase the electrical conductivity of commonly used polymers such as epoxy resin, etc. As our overall study plan is related to improvement of electrical conductivity of composite materials (mainly epoxy based composite), in this particular study, our purpose is to identify a solvent material which will have a similar

functionality as the one provided by PEO to solid polymer electrolyte. At the same time, the solvent should be compatible to epoxy resin which has oxirane group, and should not adversely influence the mechanical properties of the composite. Butyl glycidyl ether (BGE, Fig. 1) is an ether-based solvent, and has been widely used as a reactive diluent for epoxy resin. In each BGE molecule, there are two oxygen atoms which may form coordination with alkali metal ions as we found earlier in PEO molecules for improvement in the electrical conductivity of the polymer. The motion of ions in electrolyte depends on crystallinity of PEO; lower is the crystallinity, higher is the motion and therefore mechanical properties of PEO would be reduced for higher conductivity. In addition, PEO with high crystallinity would compromise the mechanical properties of structural composite materials especially of epoxy composite [18, 19].

As polymers are poor salt solvents due to their low electrical permittivity, the issue related to ion association is important. The availability of ester oxygen is a factor in ion association as the salt concentration is increased. When the amounts of solvent and salt are appropriate, salt might be dissolved completely. However, it is possible that dissolved salt is not completely dissociated into single ions only. Ion pairs, triplets, and even higher aggregates exist in equilibrium with dissociated ions. With disproportionate amounts of salt and solvent, the probability of aggregation which in fact works against the mobilization of ions, is higher. This ion clusters in the polymeric network weakens dipole orientation when there is an applied field. Dielectric relaxation studies are one approach to acquiring information related to the characteristics of molecular and ionic interactions, observation of polymeric chain mobility, and carrier generation processes in a material. Dielectric properties and electrically conductive behavior, which are highly sensitive to charged dipoles and mobile ions, are frequency dependent. It has been found that dielectric parameters were influenced by several factors such as additives, temperature, phases of materials, etc. [20–22]. Study of dielectric relaxation behavior could provide information concerning the motion of local dipole groups and dipole segments that can cause the improvement of electrical conductivity.

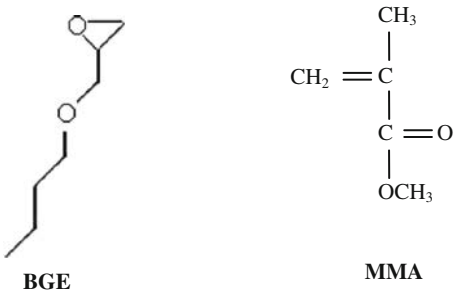

Fig. 1 Chemical structures of BGE and MMA

In this study, we investigated the mechanisms on improvement in electrical conductivity of a polymer with the addition of dissolved $LiPF_6$ in the ether-based solvent BGE. Poly (methyl-methacrylate) (PMMA) was used as base polymer due to its simplicity in preparation of the film samples. X-ray diffraction, Differential Scanning Calorimetry (DSC), and Fourier Transform Infrared Spectroscopy (FTIR) spectra studies were performed to characterize specimens to investigate the mechanisms of the conductivity improvement. Dielectric relaxation was studied to gain further insight into the ionic interaction and conductivity phenomena in the specimen.

Experiments

Sigma-Aldrich, Inc. provided PMMA with <0.5 wt.% toluene contained. Acetonitrile (CH_3CN), dissolving agent for PMMA was purchased from EM Science, a division of EM industries. Lithium hexafluorophosphate, $LiPF_6$, which was 98% pure and butyl glycidyl ether, BGE (Fig. 1), with a purity of 95% were purchased from Sigma-Aldrich, Inc.

Thin films of PMMA/$LiPF_6$ in different concentrations were prepared by solution casting technique. PMMA (5 g) was added to acetonitrile (20 mL) and stirred well to produce homogeneous viscous liquid PMMA solution. Except for drying at 70 °C in a vacuum for 24 h to remove moisture, no purification was done on $LiPF_6$. Different concentrated (0.2, 0.5, 0.75, and 1 wt.% w.r.t. PMMA) $LiPF_6$ solutions of were prepared by adding dried solid $LiPF_6$ to 4.5 mL of BGE (without any purification) separately. The PMMA solution and $LiPF_6$ solutions were mixed and stirred well. However, PMMA/$LiPF_6$ solutions with higher amounts of $LiPF_6$ showed higher viscosity and in particular, the 1 wt.% concentrated mixture was highly viscous. Measuring their viscosity was impossible since in contact with air, the mixture was solidified. A draw down bar (Paul N. Gardner Company, Inc.) was used to make thin film from PMMA/$LiPF_6$ solutions on glass substrates. The thickness of all samples was $\sim$0.09 mm. The area of the each sample (diameter = 2.50 cm) was such that it fully covered the contact surface area (diameter = 1.99 cm) of the electrical conductivity measuring instrument.

A Keithley Instrument Model 6517A with 8009 fixture was used to measure the surface resistivity of the thin films with different $LiPF_6$ wt.% by applying a voltage of 500 V DC at ambient temperature. Although the thicknesses of all samples were very close to each other ($\sim$0.09 mm), there might be differences among them on the microscale. Unlike bulk resistance, surface resistivity does not depend on

thickness and this resistivity was measured to avoid any error. More than 12 samples of each type were used for testing and each sample was tested four times changing the sample's position by turning 90° with respect to earlier position. The duration of each test was 15 min and a computer automatically collected data in 1-min intervals. X-ray diffraction measurement was done by a JEOL, JDX 8030 X-ray diffractometer to find the crystalinity of specimens. Differential scanning Calorimetry measurements were performed on samples of about 8 mg under nitrogen gas flow to a Q1000 Thermal Analysis System (TA Instruments, USA). Temperature range was 10–150 °C and heating rate was 10 °C/min. FTIR spectroscopy was used to analyze the solutions with PMMA, acetonitrile, BGE, and/or $LiPF_6$. The experiment was carried out on a Brucker IFS66 spectrometer. IR absorbance spectra were recorded in the range 400–4000 cm^{-1} and the resolution was 4 cm^{-1}.

A Novocontrol GmBH Concept 40 broadband dielectric spectrometer was used to measure the real (ε') and imaginary (ε'') parts of complex dielectric permittivity ($\hat{\varepsilon}$) at ambient temperature (298 K). This is based on alternating current (AC) system. The thin film was sandwiched between two gold plates (electrodes), one of which is spring loaded to have good contact of surface of thin film with gold plates. More than ten samples of each type were used for testing. Data were collected for the frequency range 10^{-3} to 10^{7} Hz at room temperature.

Result and discussion

Conductivity measurement

Figure 2 shows log of resistivity vs. wt.% of $LiPF_6$ diagram. Thin film with 0.75 wt.% showed the lowest resistivity with a decrease by three orders of magnitude compared to the neat PMMA thin film. From the curve of Fig. 2, it appears there are three zones to the data: zone 1 is where small amounts of additive (from 0 to 0.2 to 0.5) make only slight changes, as shown by the shallow curve reduction. Zone 2 is where a threshold seems to be reached and the resistivity drops precipitously. Zone 3 is where viscosity takes over and inhibits ion flow and that shows a higher value than zone 2. This study will attempt to identify the physical and chemical influences in each zone.

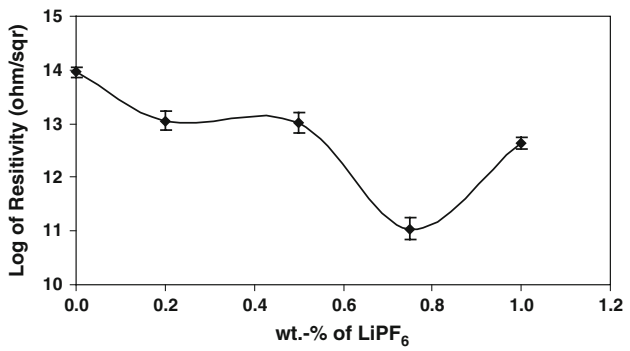

Fig. 2 Comparison of resistivity values of PMMA with different concentration of $LiPF_6$ at ambient temperature

From Fig. 2, it is seen that resistivity decreases with an increase of concentration of $LiPF_6$ up to 0.75 wt.% and then again increases beyond this point. The possible reason is a combination of both increments of Li^+ concentration and viscosity with increase of $LiPF_6$ wt.%. Beyond 0.75 wt.%, though the amount of Li^+ concentration increases, the concurrent increase of viscosity reduces the homogeneity and the mobility of Li^+ ion in the samples [23–25]. Therefore, PMMA/$LiPF_6$ solution with 0.75 wt.% $LiPF_6$ having optimum Li^+ concentration and viscosity showed the best results.

However, it is observed that specimens of 0.2 and 0.5 wt.% concentrations have around similar resistivity (Fig. 2). This phenomenon can be explained from the effect of the amount of ions and their motion in the composites. For higher conductivity, a strong network of ions is needed and for this, stoichiometric proportion of salt and media should be ideal. Deficiency of ions (in specimens of 0.2 and 0.5 wt.% concentrations) bared the formation of effective ionic links and therefore, similar conductivity results were observed. In 1 wt.%, stoichiometric aggregation and viscosity prohibited ions to form efficient links in polymer chain which resulted in lower conductivity. The conductivity depends on both concentration of charge carriers and the viscosity of the conductive substance [26, 27]. With the addition of more salt, there is an increased presence of a large number of ions in the media. This may also lead to the formation of ion aggregation which, rather than making any contribution to the conduction process, inhibits the smooth conduction process since Li^+ ions in motion would feel a repelling force from the ion aggregates [28]. Figure 2 shows that deviation of resistance in PMMA specimens is the least. The reason is that PMMA specimens were fabricated from PMMA only and the specimens were expected to be highly homogeneous. Addition of lithium salt and its dissociation result related to stoichiometric effect lessened the homogeneity of specimens and therefore deviations were likely to be higher as observed.

X-ray diffraction and DSC studies

Figure 3a–e shows the X-ray diffraction patterns of PMMA polymer and PMMA/$LiPF_6$ specimens. However, due to sensitivity to moisture, it was impossible to produce an X-ray pattern of $LiPF_6$ (also not found in literature). The broadness of the peak in the PMMA samples proves the existence of an amorphous phase and in the samples with

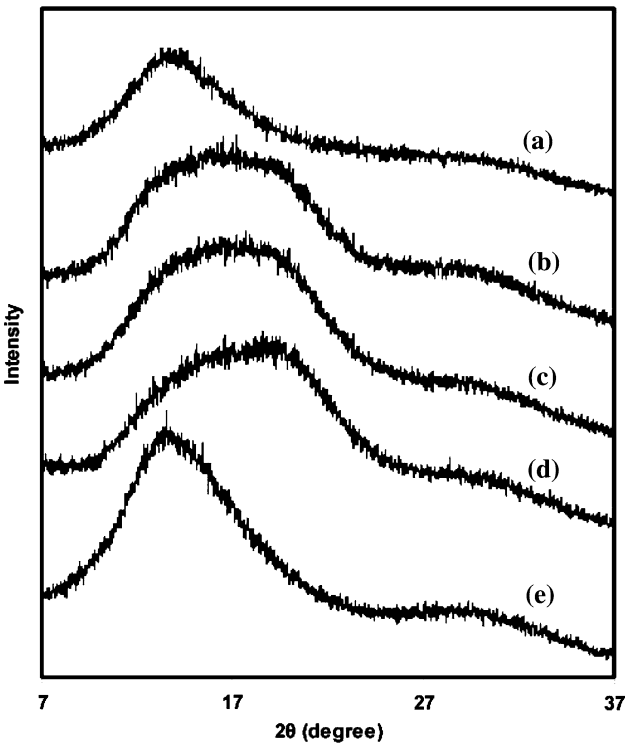

Fig. 3 X-ray diffraction pattern of (**a**) PMMA, (**b**) PMMA/$LiPF_6$ (0.2 wt.%), (**c**) PMMA/$LiPF_6$ (0.5 wt.%), (**d**) PMMA/$LiPF_6$ (0.75 wt.%), and (**e**) PMMA/$LiPF_6$ (1.0 wt.%)

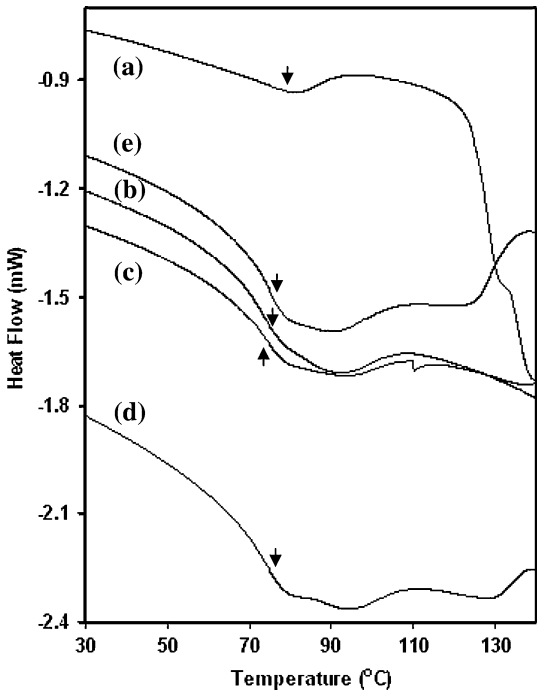

Fig. 4 DSC thermograms of (**a**) PMMA, (**b**) PMMA/$LiPF_6$ (0.2 wt.%), (**c**) PMMA/$LiPF_6$ (0.5 wt.%), (**d**) PMMA/$LiPF_6$ (0.75 wt.%), and (**e**) PMMA/$LiPF_6$ (1.0 wt.%)

$LiPF_6$ compound, the peaks are even broader. This indicates that addition of $LiPF_6$ compound increased the degree of amorphousness of the PMMA, i.e. greater disorder of the polymer chains [29]. Thus, it confirms the complete dissolution of salt in the polymer as well as the formation of homogeneous PMMA/$LiPF_6$ solutions [29]. However, the XRD pattern for the specimen containing 1 wt.% $LiPF_6$ is quite different from other $LiPF_6$-added specimens and it bears a close resemblance to the neat PMMA pattern. This phenomenon could be accounted for by the effect of viscosity at the time of preparation of the 1 wt.% specimen. The presence of Li^+ ions were not homogeneous in the 1 wt.% specimen due to the high viscosity and the ions did not come into play in changing the amorphous character of the PMMA as observed in the specimens with lower concentrations. Higher ionic conductivity originates from higher ionic diffusivity caused by the amorphous nature of the polymer. Amorphousness of the specimen with 1 wt.% $LiPF_6$ was less, i.e. less ionic diffusion, which led to lower electrical conductivity of the system.

DSC was engaged to find out the thermal behavior of PMMA/$LiPF_6$ polymer complexed system. Figure 4 shows the DSC thermograms for PMMA and PMMA/$LiPF_6$ specimens. Comparing the DSC curves of different specimens, the PMMA shows a sharp V-shaped portion ($\sim$83 °C) which can be indicative of the glass transition temperature (T_g). In the other specimens, e.g. PMMA with $LiPF_6$, T_g decreases (marked by arrow sign) and at the same time, the corresponding V-shaped part is broader. These phenomena can be explained in two ways. First, the addition of $LiPF_6$ brings more plasticity to PMMA and therefore, solid PMMA/$LiPF_6$ changes to the rubbery state at a lower temperature as compared to PMMA and this indicates that segmental motion of polymer chains becomes more flexible, which is beneficial for rapid and facile motion of Li^+ ions in PMMA. Second, the existence of the broader v-shape may also be a result of formation of a complex between PMMA and $LiPF_6$. At T_g, there is a change of state of the materials due to higher molecular motion of materials. If a complex is formed, it is possible that the bonding between different molecules and ions, and different thermal behaviors of different materials in the complex cause this broadness. This complex formation would be confirmed from FTIR analysis which has been discussed in another section later.

FTIR spectroscopy study

The infrared spectra of PMMA polymer solutions are shown in Fig. 5. There are five spectra of solutions with 0 (a), 0.20 (b), 0.50 (c), 0.75 (d), and 1.00 wt.% (e) of $LiPF_6$. If complexes are formed in crystalline or amorphous phase,

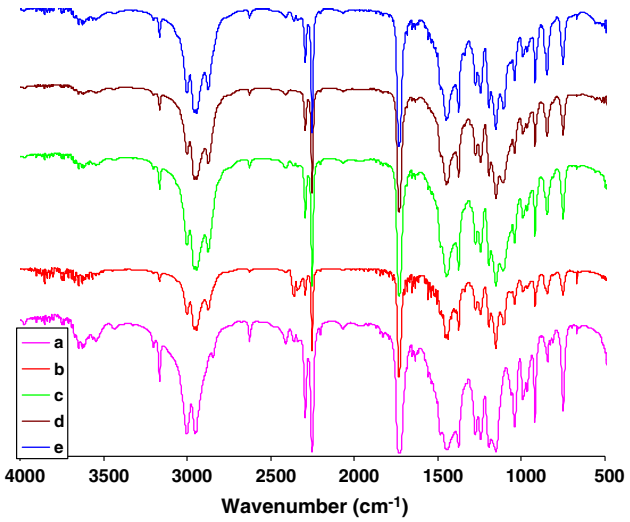

Fig. 5 FTIR plots for (**a**) PMMA, (**b**) PMMA with 0.2 wt.% $LiPF_6$, (**c**) PMMA with 0.5 wt.% $LiPF_6$, (**d**) PMMA with 0.75 wt.% $LiPF_6$, and (**e**) PMMA with 1.0 wt.% $LiPF_6$

IR would be sensitive to those. In pure PMMA, the peaks at 1728 and 2944 cm^{-1} represent C=O vibration stretching and C–H stretching, respectively. Figures 6 and 7 represent zooming views of Fig. 5, and they correspond to C=O vibration stretching and C–H stretching regions, respectively. The peak values of C=O stretching in film with 0.20 (b), 0.50 (c), 0.75 (d), and 1.00 wt.% (e) concentrations are all ~1727 cm^{-1} (Fig. 6), and this shift may not produce a big impact on electrical conductivity of PMMA. Though, other researchers did not observe any shift at 1727 cm^{-1}, they found a weak shoulder at 1700 cm^{-1} corresponding to

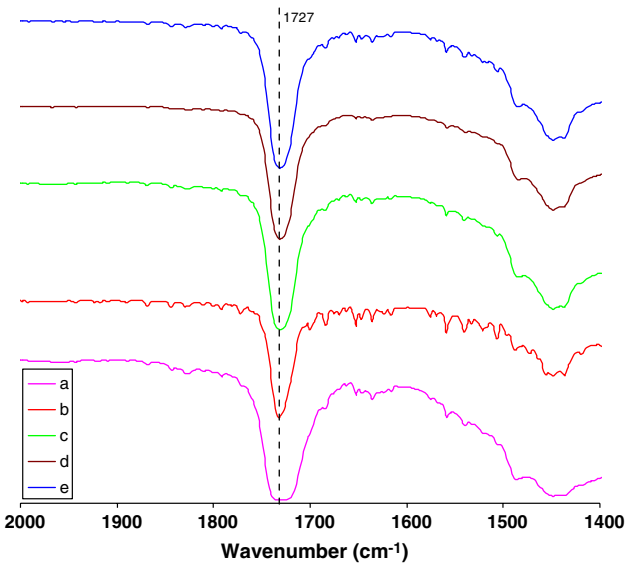

Fig. 6 FTIR plots for (**a**) PMMA, (**b**) PMMA with 0.2 wt.% $LiPF_6$, (**c**) PMMA with 0.5 wt.% $LiPF_6$, (**d**) PMMA with 0.75 wt.% $LiPF_6$, and (**e**) PMMA with 1.0 wt.% $LiPF_6$ concerned with C=O stretching vibration

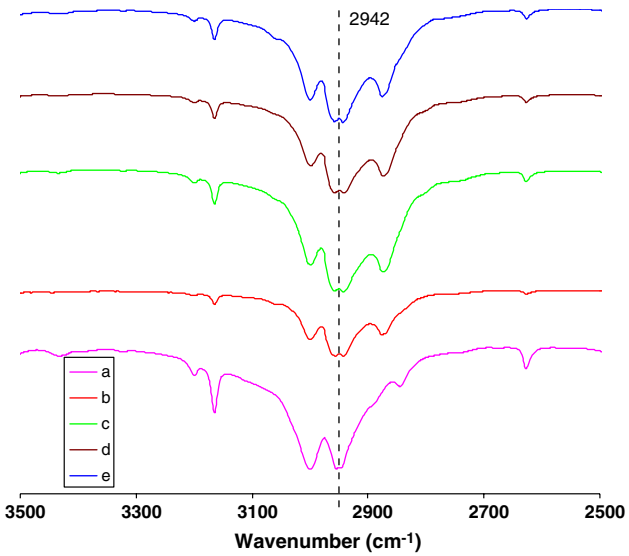

Fig. 7 FTIR plots for (**a**) PMMA, (**b**) PMMA with 0.2 wt.% $LiPF_6$, (**c**) PMMA with 0.5 wt.% $LiPF_6$, (**d**) PMMA with 0.75 wt.% $LiPF_6$, and (**e**) PMMA with 1.0 wt.% $LiPF_6$ concerned with C–H stretching

the interaction between the Li^+ and the C=O group [30, 31]. They also observed that the relative intensity of the shoulder at 1700 cm^{-1} increased with increasing the content of lithium compound. This exceptional phenomenon can be explained by the effect of complex formation between BGE and Li^+, which has been illustrated in detail later. Concerning C–H stretching, the wave numbers are around the same in specimens of different concentrations (Fig. 7). It is true that there may be some shifts of wave numbers corresponding to O–CH_2 asymmetric stretching and CH_3 asymmetric stretching of PMMA due to addition of $LiPF_6$. However, it is not our major issue in this study. We are more concerned with BGE and we want to see how it would influence the electrical conductivity of PMMA material in presence of Li salt and this is discussed in following paragraph.

FTIR spectra studies were made to analyze the molecular interactions and formation of complexes in BGE/$LiPF_6$ solutions. In Fig. 8, it is seen that the peak of the PF_6^- band splits into two peaks at ~842 and ~865 cm^{-1}. It has been found that 842 cm^{-1} is associated with free PF_6^- anions [28] and 865 cm^{-1} is expected to be attributed to the presence of Li^+–PF_6^- contact ion pairs (however, it cannot be confirmed as the band for Li^+–PF_6^- contact ion pairs was not available in any report). Similar observations were reported by [28, 32] though with different kinds of salt used in their experiments. Comparing the curves in Fig. 8, it can be observed that the characteristic peak of free PF_6^- becomes sharp with the disappearance of Li^+–PF_6^- contact ion pairs peak for the solution with 0.75 wt.% $LiPF_6$. Therefore, it can be confirmed from this analysis that among all the BGE/$LiPF_6$ solutions, the greatest amount of

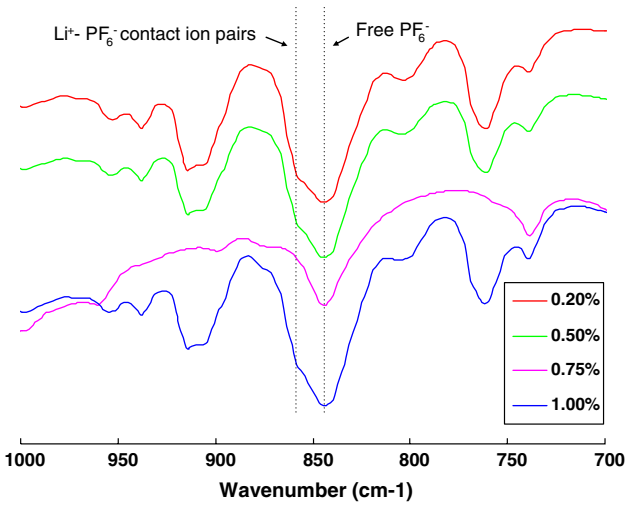

Fig. 8 FTIR plots for BGE–$LiPF_6$ complexes with different amount of $LiPF_6$ concerned with PF_6^- and Li^+–PF_6^- contact ion pairs

ionization occurred in the solution with 0.75 wt.% $LiPF_6$, which is beneficial for the release of Li^+. However, it is surprising that both broad curve at 842 cm^{-1} and weak shoulder at 865 cm^{-1} are seen in the FTIR spectra for the solutions with 0.20 and 0.50 wt.% $LiPF_6$ as the amount of BGE in these two solutions was more than the requirement for full dissociation of $LiPF_6$ salt. More research needs to be done to find the reasons for this occurrence.

The band at 1108 cm^{-1} corresponds to C–O stretching vibration in BGE. In different BGE–$LiPF_6$ complexes with 0.20, 0.50, 0.75, and 1.00 wt.% of $LiPF_6$, peaks corresponding to C–O stretching vibration shifted to 1108, 1110, 1117, and 1112 cm^{-1}, respectively, as shown in Fig. 9. Of special note, we found shifting of the peak from 1108 to 1117 cm^{-1} accompanied with broadening in BGE–$LiPF_6$ complexes with 0.75 wt.% of $LiPF_6$. As mentioned earlier that only 0.75 wt.% contained proportionate stoichiometric amount of BGE and $LiPF_6$ to produce a good complex. In all other specimens, either excess amount of BGE or excess amount of $LiPF_6$ might have reduced the effect of complex.

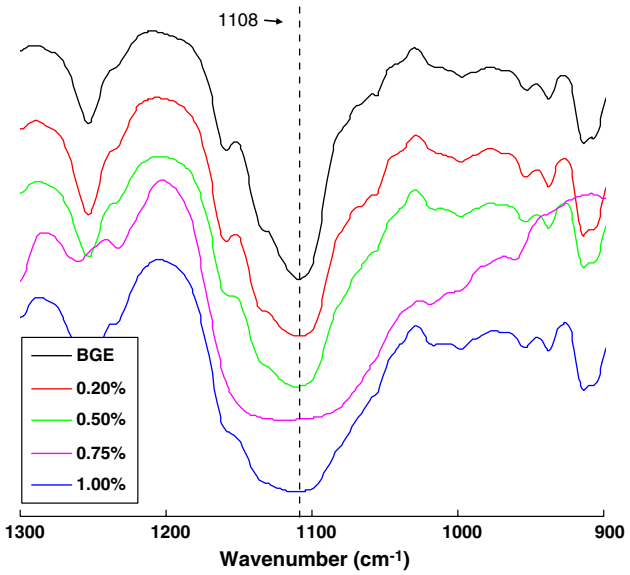

Fig. 9 FTIR plots for BGE–$LiPF_6$ complexes with different amount of $LiPF_6$ concerned with C–O stretching vibration

In Glycidyl ethers, 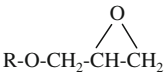 , where R is an alkyl or an aryl group, there are two kinds of ether bond: one is linear and the other is cyclic. As a nucleophile attack to the less hindered carbon atom is most favorable, the scission of strained cyclic oxirane ring occurs through opening in the β-position, i.e. between the CH_2 group and oxygen under basic condition [33]. Another formation of a peak at 3400 cm^{-1} was found distinctly in the BGE–$LiPF_6$ complex with 0.75 wt.% $LiPF_6$ (Fig. 10). This peak corresponds to the absorption of hydroxyl (OH) units. The possible reason is the oxygen ring opening in BGE (Fig. 1) due to the presence of Li^+ of $LiPF_6$, and this oxygen formed hydroxyl unit, which changed the polarity of the complex, helped in improving the electrical conductivity (zone 2). On the other hand, $LiPF_6$ can easily absorb water and therefore absorption of water cannot be dismissed fully, even though utmost care was taken in sample preparation and experiment. The hydroxyl absorption shown in Fig. 10 might be attributed to absorption of trace water to some extent. Accordingly, in the sample with 1 wt.% $LiPF_6$, there was a probability of higher amounts of water absorption compared to samples with 0.75 wt.% $LiPF_6$, and therefore hydroxyl absorption for the 1 wt.% PMMA/$LiPF_6$ sample would be more prominent compared to the 0.75 wt.% PMMA/$LiPF_6$ sample as all samples were prepared under similar processing conditions. However, from Fig. 10, this phenomenon is not observed.

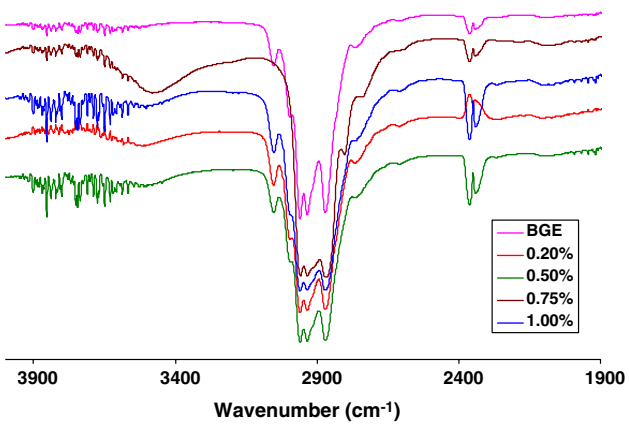

Fig. 10 FTIR plots for BGE–$LiPF_6$ complexes with different amount of $LiPF_6$ concerned with absorption of hydroxyl (OH) unit

Even the sample with 0.5 wt.% $LiPF_6$ does not have prominent hydroxyl absorption as much as the sample with 0.75 wt.% $LiPF_6$. Therefore, the suggestion of complex formations between BGE and $LiPF_6$ through oxygen ring opening is strengthened. Additionally, in another BGE–$LiPF_6$ complex (0.2 wt.%), absorption of hydroxyl units is not obviously prominent. In 0.2 and 0.5 wt.%, it may be possible that the stoichiometric proportion of BGE and $LiPF_6$ was such that all the oxygen rings were not opened and in 1 wt.%, over concentration of $LiPF_6$ caused the increment of viscosity and nonhomogeneity of the solution might have lessened the effect of opened rings in formation of hydroxyl unit. However, unlike BGE specimens, specimens with 0.2, 0.5, and 1.0 wt.% $LiPF_6$ show the peaks of hydroxyl absorption to some extent (Fig. 10).

The above-discussed ring opening can be confirmed from FTIR spectra as shown in Fig. 11. The band attributed to oxirane group 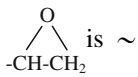 is ~910 [34]. In the presence of $LiPF_6$ salt (0.75 wt.%) in BGE, the oxirane peak vanishes. This means that there is a ring opening in the oxirane group by the presence of Li^+ ion and the oxygen may react with hydrogen to form hydroxyl ions as observed in other FTIR spectrum. However, this ring opening in other solutions (0.20 and 0.50 wt.%) was not prominent. The possible cause is that the amount of Li^+ ion is less compared to the amount of oxirane groups available in the solution. In the case of 1 wt.% solution, although Li^+ ions are high in concentration, it is feasible that their aggregation (as discussed earlier) and high viscosity would have barred them from effective ring opening. In addition, there is a disappearance of some other peaks (Fig. 11) which occurs mainly for the solution with 0.75 wt.% $LipF_6$ which needs more research to find out effect of $LipF_6$ on BGE.

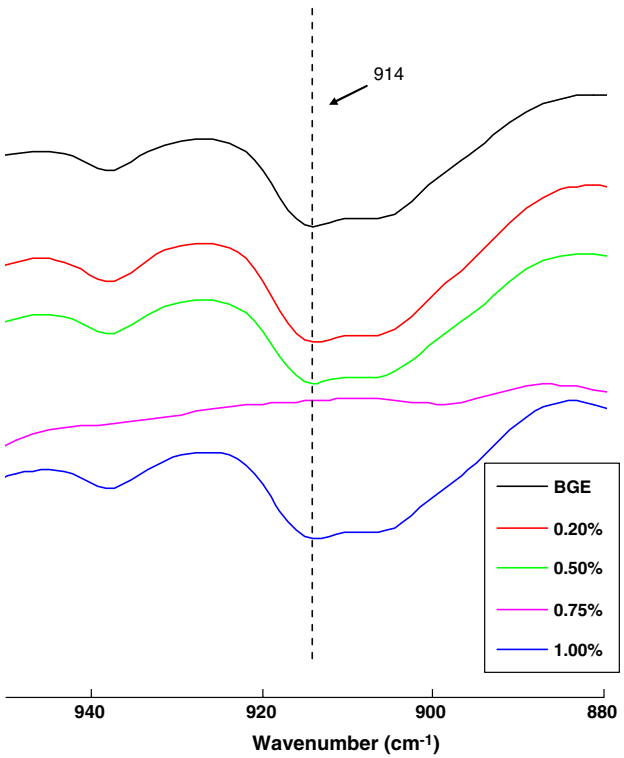

Fig. 11 FTIR plots for BGE–$LiPF_6$ complexes with different amount of $LiPF_6$ concerned with oxirane group

This complex formation between BGE and $LiPF_6$ has an effect on the total PMMA/BGE/$LiPF_6$ solution. Since $LiPF_6$ already made a complex with BGE through Li^+, a lesser number of Li^+ ions were available to make any complex with the C=O group of PMMA when the BGE/$LiPF_6$ solution was mixed compared to pure PMMA. In other words, this phenomenon might have subdued the formation of any kind of complex between the C=O group of PMMA and Li^+ of $LiPF_6$, which were observed in other researchers work with a weak shoulder at 1700 cm^{-1} [30, 31] as mentioned earlier. In preparation of the samples, the $LiPF_6$ compound was dissolved in BGE and therefore, most of the Li^+ of $LiPF_6$ were engaged with BGE, and the remainder, which might make any complex with C=O group of PMMA, were not enough to cause a shoulder at 1700 cm^{-1}.

From FTIR analysis, it is found that $LiPF_6$ played the main role with assistance from BGE in improvement of electrical conductivity. Irrespective of the polymer we can implement this system, which is important for practical application of many polymer materials. We expect that it would also be demonstrated in an epoxy resin system which has oxirane groups as BGE has and this extra presence of oxirane group might help in better dissociation of $LiPF_6$. This is the subject of our future study.

Dielectric studies

Theory

Complex dielectric constants (ε^*) consists of relative permittivity constant or dielectric constant (ε' or *permitivity'*) and relative loss permittivity or dielectric loss (ε'' or *permitivity''*) as shown below:

$$\varepsilon^* = \varepsilon' - i\varepsilon'' \quad (1)$$

where ε' and ε'' depend on frequency of the applied field. When an electrical field is applied to a material, the dipoles in the material show the tendency to orient them in the direction of the applied field. However, mobilization of the dipole depends on the ductility of the materials. At higher temperatures, dipoles can orient easily whereas a highly crosslinked material finds difficulty in orientation. The delayed response to a stimulus in a system is the so-called relaxation. The orientation involves a characteristic time

called relaxation time (γ). Relaxation can be local (β, γ) or segmental (α). The higher the value of ε' the better is the electrical conductivity. ε'' measures the energy loss due to orientation of dipoles; and energy loss due to conduction of ionic species in the material when an electrical field applied. The ratio of ε' and ε'' is known as the loss tangent or dissipation (tan δ):

$$\tan\ \delta = \varepsilon'/\varepsilon'' \tag{2}$$

To describe the way the molecule behaves in response to the applied field, the Debye relaxation model has been widely used and it is [35]:

$$\varepsilon^*(\omega) = \varepsilon_\alpha + \frac{\varepsilon_0 - \varepsilon_\alpha}{1 + (i\omega\tau)} \tag{3}$$

ε_0 is the zero-frequency dielectric constant, ε_α the limiting high-frequency dielectric constant, ω the average angular frequency, and $i = \sqrt{-1}$. The Debye model generally is used where dipoles can be rotated in viscous fluid [36]. However, Cole–Cole model [35], which is expressed in Eq. 4, has been made to explain other viscous relaxation process.

$$\varepsilon * (\omega) = \varepsilon_\alpha + \frac{\varepsilon_0 - \varepsilon_\alpha}{1 + (i\omega\tau)^\alpha} \tag{4}$$

The range of α which is the parameter to signify the breadth of experimental relaxation peaks is between 0 and 1. ε'' vs. ε' plot is called the Cole–Cole dielectric constant diagram. A Cole–Cole diagram of the Debye model would be semicircle and the center of it would lie on ε' axis whereas the diagram for its model is a skewed arc. From the ε'' vs. ε' plot, maximum loss would be obtained for a particular frequency (which is called $\omega_{\max}$). The relaxation time γ can be obtained from the relation:

$$\omega_{\max} = 1/\tau \tag{5}$$

The relaxation process could be further investigated by use of the complex electric modulus M. It gives insight into the bulk properties and is effective to describe the dielectric response of nonconducting materials. For vitreous ionic conductors as well as for polycrystalline ceramics, this modulus is useful in the analysis of relaxation properties. The relation between M and $\varepsilon*$ are as followed:

$$M = \frac{1}{\varepsilon} = M' + M'' \tag{6}$$

$$M' = \frac{\varepsilon'}{\varepsilon'^2 + \varepsilon''^2} \tag{7}$$

$$M'' = \frac{\varepsilon''}{\varepsilon'^2 + \varepsilon''^2} \tag{8}$$

The complex modulus depends both on ε' and ε'', and therefore, data analysis with it would be more robust.

Behavior

Dielectric behaviors of pure PMMA and PMMA/$LiPF_6$ specimens were observed in terms of variation of frequency. Figure 12 shows the variation of dielectric constant (ε') with frequency. Similar behavior was reported in a number of papers [37, 38]. While performing dielectric measurement on materials, there is a contribution from dipoles as well as mobile ions to the relative permittivity of the materials. It is obvious that variation of curves occurs due to the presence of various amounts of $LiPF_6$ as amounts of other components were fixed in the samples. It was observed from the figure that with increase of frequency, the dielectric constant decreases for PMMA/$LiPF_6$ film and reaches a constant value at about 10^4 Hz. The dielectric constant decreases rapidly in the range of 10^{-2} to 1 Hz. With increases to the $LiPF_6$ loading in PMMA, ε' shows a strong step-like increase (in frequency range 10^2 to 10^4) which increases with further lowering of the frequency. The step shifts corresponding to $LiPF_6$ loading in PMMA show the typical signature of relaxational behavior. At low frequency, dipoles are able to follow an oscillating electric field more easily than at a high frequency at a given temperature. This may endorse the phenomena that at low frequency range, the dipoles of macromolecules tend to reorient themselves in the direction of applied field, whereas the dipoles may not be able to reorient themselves in the direction of applied field in high frequency range, and thus, in the high frequency range, the dielectric constant decreases [39]. Another possible explanation could be attributed to development of a space charge at the interface between electrode and film. This is known as non-Debye behavior. Ion diffusion plays an important role in space charge generation with respect to frequency [40]. At low frequency, contribution of accumulated charges is prominent at the interface whereas with increasing frequency, input from charge carriers decreases due to high periodic

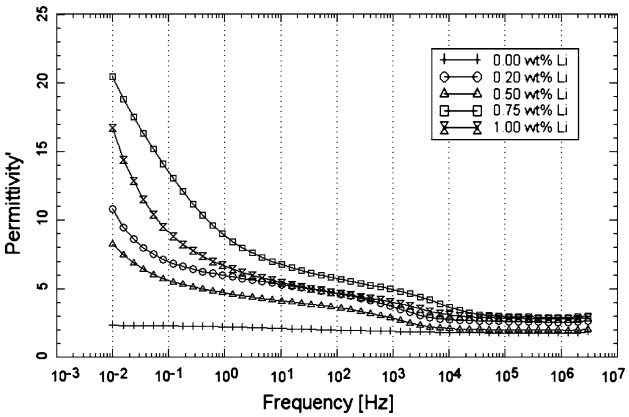

Fig. 12 Variation of dielectric constant (ε') with frequency of pure PMMA and PMMA–$LiPF_6$ complexes

reversal of the field at the interface [41]. At a particular frequency, the value of dielectric constant is higher in PMMA–$LiPF_6$ complexes compared to that in pure PMMA, and the highest value is in specimen with 0.75 wt.% $LiPF_6$. This can be explained with consideration of increased number of dipoles and decreased in relaxation times due to addition of $LiPF_6$. However, specimens with 1 wt.% $LiPF_6$ show lower dielectric constant due to high viscosity of the liquid mixture at the time of sample preparation which retards the well formed and distributed dipoles throughout the sample.

Dielectric loss (ε'') vs. frequency curves as shown in Fig. 13 depict that with increase of frequency, the value of dielectric loss decreases, and finally at frequency around 10 Hz it reaches a constant value. Addition of $LiPF_6$ caused the high dielectric loss in PMMA–$LiPF_6$ complexes compared to pure PMMA. These high dielectric losses in complex films cause the increase of electrical conductivity of the related specimens. Specimens with higher heterogeneity correspond to greater dielectric loss. Though the peaks in dielectric loss (ε'') vs. frequency curves (Fig. 13) of Li salt-included specimens are not prominent, they are obvious in the tan δ vs. frequency curves (Fig. 14) which corresponds to the relaxation process. In the range of 10^3–10^5 Hz, PMMA–$LiPF_6$ complexes show β relaxation as dielectric observation in specimens that were tested at 25 °C, much below the glass transition temperature (105 °C). This relaxation can be attributed to the changes of orientation of polar group C–O, a bond dipole in BGE. However, in pure PMMA, β relaxation is not prominent (Fig. 14). The shift of β relaxation in the specimen with 0.75 wt.% $LiPF_6$ toward a high frequency (10^4 Hz) denotes an accelerated relaxation and decrease in relaxation time. In other specimens, stoichiometric effects may result in an aggregation or deficiency of ions and their reduced

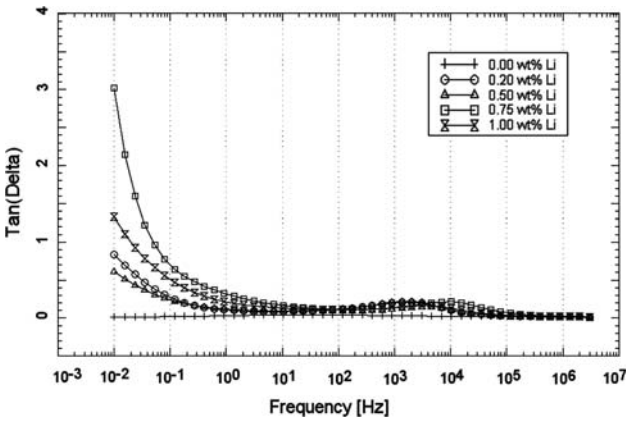

Fig. 14 Variation of tan(δ) with frequency of pure PMMA and PMMA–$LiPF_6$ complexes

mobilization. This may obstruct the orientation of dipoles, i.e. causing a higher relaxation time.

Dielectric relaxation experiments at different frequencies also provide the information regarding relaxation times, possible relaxators and their activation energy. The Cole–Cole plot is a good way to study relaxation mechanisms in PMMA and its complexes. Figure 15 show the dielectric Cole–Cole diagrams (which are originally ε'' vs. ε' diagrams) of the systems with different $LiPF_6$ content (only arc part of ε'' vs. ε' curves has been considered and it is up to the frequency of 10^6 Hz). It was found that beyond the frequency of 10^6 Hz, the curvature of the plot was changing toward the opposite direction in each specimen. The plots (Fig. 15) indicate that each arc except the arc for PMMA is a part of a circle whose center lies below the ε' axis. The relaxation in specimens was dominated by the Cole–Cole model. It may be observed from the figure that addition of $LiPF_6$ compound to PMMA changes the arc toward the semicircle and it is prominent in the specimen

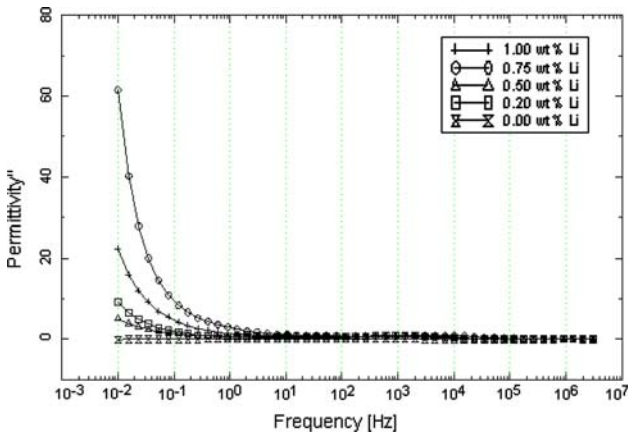

Fig. 13 Variation of dielectric loss (ε'') with frequency of pure PMMA and PMMA–$LiPF_6$ complexes

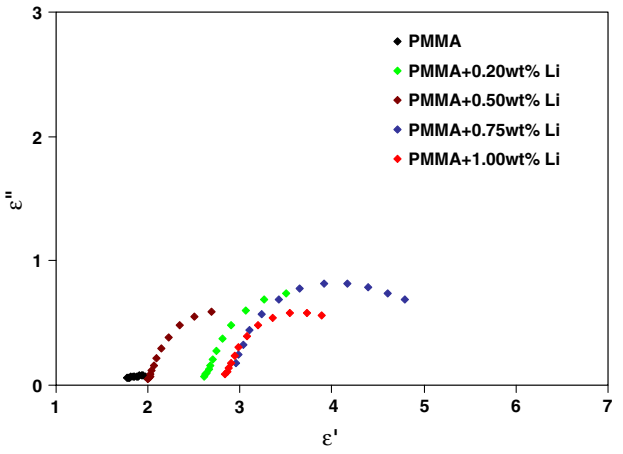

Fig. 15 Dielectric Cole–Cole diagrams of the systems with different wt.% of $LiPF_6$ in PMMA

Table 1 Relaxation time of different type of specimens

Specimen type	Relaxation time (γ) (in s)
PMMA + 0.20 wt.% $LiPF_6$	1.10×10^{-3}
PMMA + 0.50 wt.% $LiPF_6$	7.79×10^{-4}
PMMA + 0.75 wt.% $LiPF_6$	2.18×10^{-4}
PMMA + 1.00 wt.% $LiPF_6$	3.28×10^{-4}

with 0.75 wt.% Li compound. Therefore, this specimen shows more monodispersive nature of the dielectric properties. The calculated values of γ for all the specimens except PMMA specimen have been listed in Table 1. The least relaxation time is found in specimen with 0.75 wt.% $LiPF_6$.

However, in modulus loss spectrum (M'' vs. frequency) (Fig. 16), there are two M'' maxima in each curve. One of them is related to high frequency β relaxation as discussed earlier and other should be low frequency β relaxation process. Though the relaxation in pure PMMA was not observed in tan δ vs. frequency diagram (Fig. 13), in Fig. 16, there is one peak for PMMA. This might be a relaxation process whose origin is the partial rotation of the $-COOCH_3$ side groups around the C–C bonds linking these side groups to the main chain. Dielectric measurement temperature (25 °C) was below the T_g (97.28 °C, observed in our experiment) and therefore, it was impossible to have α relaxation process.

At low frequency, high values of permittivity and loss were detected which could be influenced by the presence of electrode polarization as observed by other researchers [42–45]. However, the researchers found very minor polarization at low temperature and low frequency. Larger amount polarization was identified at temperature higher than glass transition temperature of the material where the material would be viscous. In liquid sample, effects of polarization are prominent too [45–47]. In our study, all the experiments were performed on solid samples at room temperature (25 °C) temperature which was far below T_g of pure PMMA (~83 °C) and therefore, apparently, it can be said that influence of electrode polarization was less. Moreover, at the low frequency, the values of permittivity and loss were so high that electrode polarization influence could be step aside. However, complete view of this influence on our sample could be obtained using some existing models which is our future work [45].

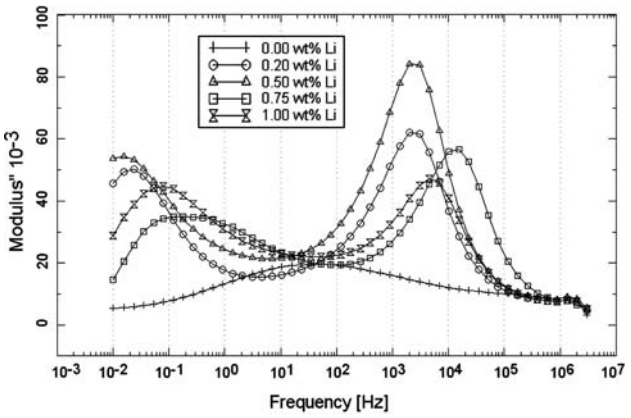

Fig. 16 Modulus diagram of pure PMMA and PMMA–$LiPF_6$ complexes

Conclusions

Improvement in electrical conductivity of the PMMA/$LiPF_6$ was obtained through dissolving PMMA and $LiPF_6$ in acetonitrile and BGE, respectively. It is found that the prepared thin film with 0.75 wt.% $LiPF_6$ showed the highest conductivity value with the improvement of electrical conductivity by three orders of magnitude compared to pure PMMA film. The possible reason for the behaviors of specimens of other concentration is disproportionate stoichiometry and its related effects. XRD and FTIR spectra were utilized to study the mechanism, which confirmed the formation of BGE–$LiPF_6$ complexes. Due to the presence of $LiPF_6$ in BGE solution, there was a ring opening and formation of OH group and Li^+ which changed the polarity of the solution. There were also spectra changes of C–O stretching motion band which occur upon addition of $LiPF_6$. Dielectric experiments reveal the existence of multiple composition-dependent relaxation processes. The β process is associated with C–O group present in BGE. The β' relaxation tends to appear at low frequency and corresponds to $-COOCH_3$ side groups of PMMA. The study results indicated that BGE can cause the lithium compound to improve the electrical conductivity of a polymer at very low concentrations of the lithium compound without the existence of solid fillers in the polymers.

This work also suggests that the conductivity of nanocomposites with various solid conductive fillers, which is the subject of much hectic current work, and is as yet inadequate for many applications including aerospace, may be sufficiently enhanced in combination with this ion conduction approach involving a "liquid conductive filler." Since BGE is compatible with epoxy molecules, further study is expected to result in a combination of electronic and ionic conduction as the nearer-term solution to conductive epoxy composites in their wide field of applications in aircraft, energy and electronics component industries. Further, this work suggests a foundation for the development of structural batteries, which require multi-functional materials for their electrolytes.

Acknowledgements The authors are very grateful to Mr. Russell G. Maguire of the Boeing Company for fruitful discussions on this work. The authors gratefully acknowledge the support from NSF through NIRT grant 0506531. This work is also partially supported by NASA through grant NNM04AA62G.

References

1. Kovacs JZ, Velagala BS, Schulte K, Bauhofer W (2007) Comp Sci Technol 67:922. doi:10.1016/j.compscitech.2006.02.037
2. Dalmas F, Cavaille JY, Gauthier C, Chazaeau L, Dendievel R (2007) Comp Sci Technol 67:829. doi:10.1016/j.compscitech.2006.01.030
3. Saikia D, Kumar A (2005) Euro Polym J 41:563. doi:10.1016/j.eurpolymj.2004.10.029
4. Trangaris GM, Psarras GC, Kouloumbi N (1998) J Mater Sci 33:2027. doi:10.1023/A:1004398514901
5. Rajendran S, Sivakumar P, Babu RS (2007) J Power Sour 164:815. doi:10.1016/j.jpowsour.2006.09.011
6. Wang HX, Wang ZX, Li H, Meng QB, Chen LQ (2007) Electrochim Acta 52:2039. doi:10.1016/j.electacta.2006.08.013
7. Uma T, Mahalingam T, Stimming U (2005) Mater Chem Phys 90:239. doi:10.1016/j.matchemphys.2003.11.010
8. Lee SH, Cho KI, Choi JB, Shin DW (2006) J Power Sour 162:1341. doi:10.1016/j.jpowsour.2006.07.061
9. Morales E, Acosta JL (1999) Electrochim Acta 45:1049. doi:10.1016/S0013–4686(99)00300-X
10. Cazzanelli E, Croce F, Appetecchi B, Benevelli F, Mustarelli P (1997) J Chem Phys 107:5740. doi:10.1063/1.474334
11. Croce F, Sacchetti S, Scrosati B (2006) J Power Sour 161:560. doi:10.1016/j.jpowsour.2006.03.069
12. Wintersgill MC, Fontanella JJ, Stallworth PE, Newman SA, Chung SH, Greenbaum SG (2000) Solid State Ionics 135:155. doi:10.1016/S0167–2738(00)00295–2
13. Jeon BH, Yeon JH, Chung JJ (2003) J Mater Process Technol 143–144:93. doi:10.1016/S0924-0136(03)00327-3
14. Bendler JT, Fontanella JJ, Shlesinger MF, Wintersgill MC (2001) Electrochimica Acta 46:1615. doi:10.1016/S0013-4686(00)00761-1
15. Castillo J, Delgado I, Chacón M, Vargas RA (2001) Electrochimica Acta 46:1695. doi:10.1016/S0013-4686(00)00772-6
16. Basak P, Manorama SV (2004) Euro Polym J 40:1155. doi:10.1016/j.eurpolymj.2004.01.013
17. Kurian M, Galvin ME, Trapa PE, Sadoway DR, Mayes AM (2005) Electrochim Acta 50:2125. doi:10.1016/j.electacta.2004.09.020
18. Ramesh S, Winie T, Arof AK (2007) Euro Polym J 43:1963. doi:10.1016/j.eurpolymj.2007.02.006
19. Huang YP, Woo EM (2001) Polymer 42:6493. doi:10.1016/S0032-3861(01)00114-8
20. Cho CW, Cho YS, Yeo JG, Kim J, Paik U (2003) J Euro Ceram Soc 23:2315. doi:10.1016/S0955-2219(03)00087-6
21. Vaughan AS, Zhao Y, Barré LL, Sutton SJ, Swingler SG (2003) Euro Polym J 39:355. doi:10.1016/S0014-3057(02)00194-5
22. Yang S, Benitez R, Fuentes A, Lozano K (2007) Comp Sci Technol 67:1159. doi:10.1016/j.compscitech.2006.05.022
23. Tambelli CE, Donsco JP, Magon CJ, Pereira EC, Rosario AV (2007) Electrochim Acta 53:1535. doi:10.1016/j.electacta.2007.05.008
24. Tsunashima K, Yonekawa F, Sugiya Masashi S (2008) Chem Lett 37:314. doi:10.1246/cl.2008.314
25. Krouse D, Guo Z, Kranbuehl DE (2005) J Non-Crystal Solids 351:2831. doi:10.1016/j.jnoncrysol.2005.03.053
26. Battisti D, Nazri GA, Klassen B, Aroca R (1993) J Phys Chem 97:5826. doi:10.1021/j100124a007
27. Southall JP, Hubbard HV, Johnston F, Rogers V, Davies GR, Mcintyre JE, Ward IM (1996) Solid State Ionics 85:51. doi:10.1016/0167-2738(96)00040-9
28. Sharma JP, Sekhon SS (2006) J Mater Sci 41:3617. doi:10.1007/s10853-006-6317-1
29. Shanmukaraja D, Wanga GX, Muruganc R, Liua HK (2008) J Phys Chem Solid 69:243. doi:10.1016/j.jpcs.2007.08.072
30. Chiu CY, Yen YJ, Kuo SW, Chen HW, Chang FC (2007) Polymer 46:1329. doi:10.1016/j.polymer.2006.12.059
31. Chen HW, Lin TP, Chang FC (2002) Polymer 43:5281. doi:10.1016/S0032-3861(02)00339-7
32. Tang Z, Wang J, Chen Q, He W, Shen C, Mao X, Zhang J (2007) Electrochim Acta 52:6638. doi:10.1016/j.electacta.2007.04.062
33. Morrisson MT, Boyd RN (1987) Organic chemistry. Allyn and Bacon, Boston MA, p 721
34. Yuan L, Liang G, Xie J, Li L, Guo J (2006) Polymer 47:5338. doi:10.1016/j.polymer.2006.05.051
35. Cole KS, Cole RH (1969) J Chem Phys 1:341
36. Chelkowski A (1980) Dielectric physics. Elsevier Scientific Publisher Company, Amsterdam
37. Natesan B, Karan NK, Rivera MB, Aliev FM, Katiyar RS (2006) J Non-Crystal Solid 352:5205. doi:10.1016/j.jnoncrysol.2006.01.138
38. Eliasson H, Albinsson I, Mellander BE (1998) Electrochim Acta 43:1459. doi:10.1016/S0013-4686(97)10084-6
39. Reicha FM, El-Hiti M, El-Sonabati AZ, Diab MA (1991) J Phys D Appl Phys 24:369. doi:10.1088/0022-3727/24/3/020
40. Macdonald JR (ed) (1987) Impedance spectroscopy. Wiley, New York
41. Mark HF (ed) (1964) Ency. of polymer science and engineering, vol 1. Wiley-Interscience Publication, Wiley, New York
42. Yoshimi S, Matsui T, Kikuchi R, Eguchi K (2008) J Power Sour 179:497. doi:10.1016/j.jpowsour.2008.01.003
43. Lu H, Zhnag X, He Bo, Zhang H (2005) J Appl Polym Sci 102:3590. doi:10.1002/app.23987
44. Steeman PAM, Maurer FHJ (1992) Polymer 33:4236. doi:10.1016/0032-3861(92)90263-V
45. Pathmanathan K, Johari GP (1993) J Polym Sci B Polym Phys 31:265. doi:10.1002/polb.1993.090310304
46. Bykova Z, Klugman I, Sorkin YI (1980) Measure Tech 23:936. doi:10.1007/BF00825286
47. Mirtaheri P, Grimnes S, Martinsen OG (2005) IEEE Trans Biomed Eng 52:2093. doi:10.1109/TBME.2005.857639